HIROSHIMA MATH. J.
43 (2013), 179–206

Semi-exact equilibrium solutions for three-species competition-diffusion systems

Chiun-Chuan CHEN, Li-Chang HUNG, Masayasu MIMURA,
Makoto TOHMA and Daishin UEYAMA

(Received March 1, 2012)
(Revised April 23, 2012)

ABSTRACT. We consider a three-species competition-diffusion system, in order to discuss the problem of competitor-mediated coexistence in situations where one exotic competing species invades a system that already contains two strongly competing species. It is numerically shown that, under some conditions, there exist stable non-constant equilibrium solutions that indicate the coexistence of two strongly competing species. This result motivates us to develop a semi-exact representation for finding these equilibrium solutions from an analytical viewpoint.

1. Introduction

Species diversity in ecological communities is currently investigated not only through field research but also from a theoretical standpoint. A particularly important line of inquiry in this field is the coexistence of species mediated by the impact of invaders, food, body sizes, and dispersal ([4], [7], [12]). A simple but representative example is competitor-mediated coexistence among three biological species (say U, V and W), where one exotic species (W) invades a system in which the other two (U and V) are already strongly competing. This competitor-mediated coexistence of U and V in the presence of W can be theoretically modeled by the following three-species competitive Lotka–Volterra system:

$$\begin{cases} u_t = (r_1 - a_1 u - b_{12} v - b_{13} w)u, \\ v_t = (r_2 - b_{21} u - a_2 v - b_{23} w)v, \\ w_t = (r_3 - b_{31} u - b_{32} v - a_3 w)w, \end{cases} \qquad t > 0, \tag{1}$$

The first author is partly supported by the NCS (Taiwan) grant 100-2115-M-002-009-MY2.

The third, fourth and fifth author are supported by KAKENHI S (No. 18104002) and the Global COE program (G14) 'Formation and Development of Mathematical Science based on Modeling and Analysis'.

2010 *Mathematics Subject Classification.* Primary 35K57; Secondary 92D40.

Key words and phrases. reaction-diffusion equations, competitor-mediated coexistence, semi-exact equilibrium solutions.

where $u(t)$, $v(t)$ and $w(t)$ denote the population densities of U, V and W at time t, respectively. The parameters r_i, a_i and b_{ij} $(i, j = 1, 2, 3\ (i \neq j))$ represent the intrinsic growth rates, intra-specific competition rates and inter-specific competition rates, respectively, which are all positive constants.

We consider (1) with the initial conditions

$$u(0) = u_0 > 0, \qquad v(0) = v_0 > 0, \qquad w(0) = w_0 > 0. \tag{2}$$

We first impose the following assumption on the interaction of the two pre-existing competing species U and V in the absence of W:

(A1) $\frac{b_{12}}{a_2}, \frac{a_1}{b_{21}} < \frac{r_1}{r_2}$.

This implies that for the (u, v) system satisfying

$$\begin{cases} u_t = (r_1 - a_1 u - b_{12} v)u, \\ v_t = (r_2 - b_{21} u - a_2 v)v, \end{cases} \qquad t > 0, \tag{3}$$

the equilibrium point $\left(\frac{r_1}{a_1}, 0\right)$ is stable, whereas $\left(0, \frac{r_2}{a_2}\right)$ is unstable; that is, U always survives and V becomes extinct. In other words, *absolutely competitive exclusion* occurs between U and V.

We now consider the situation where W invades the (U, V) system. The natural question is, 'Is it possible for U and V to coexist in the presence of W?' If the parameters in (1) are specified in such a way that a positive equilibrium point (say (u^*, v^*, w^*)) exists and is stable, and other equilibrium points are unstable, then the answer is obviously in the affirmative.

In this paper, we assume the following condition for (1):

(A2) In addition to the stability of (u^*, v^*, w^*), $(r_1/a_1, 0, 0)$ is also stable and other equilibrium points are unstable, even if they exist.

In order to explain (A2) more precisely, we make the following assumptions on the interactions between U and W as well as between V and W:

(A3) $\frac{a_1}{b_{31}} < \frac{r_1}{r_3} < \frac{b_{13}}{a_3}$.

This implies that for the (u, w) system satisfying

$$\begin{cases} u_t = (r_1 - a_1 u - b_{13} w)u, \\ w_t = (r_3 - b_{31} u - a_3 w)w, \end{cases} \qquad t > 0, \tag{4}$$

both $\left(\frac{r_1}{a_1}, 0\right)$ and $\left(0, \frac{r_3}{a_3}\right)$ are stable, while a positive equilibrium point (say $(\breve{u}, \breve{w})$) is unstable; that is, *strong competition* exists between U and W.

(A4) $\frac{b_{23}}{a_3} < \frac{r_2}{r_3} < \frac{a_2}{b_{32}}$.

This implies that for the (v, w) system satisfying

$$\begin{cases} v_t = (r_2 - a_2 v - b_{23} w)v, \\ w_t = (r_3 - b_{32} v - a_3 w)w, \end{cases} \qquad t > 0, \tag{5}$$

both $\left(\frac{r_2}{a_2}, 0\right)$ and $\left(0, \frac{r_3}{a_3}\right)$ are unstable, while a positive equilibrium point (say $(\hat{v}, \hat{w})$) is stable; that is, *weak competition* exists between V and W, allowing them to coexist.

If the initial value of $(u(0), v(0), w(0))$ lies in the neighborhood of (u^*, v^*, w^*), (A2) indicates that competitor-mediated coexistence occurs for U and V in (1) and (2). However, if $(u(0), v(0), w(0))$ does not satisfy this condition, the behavior of solutions $(u(t), v(t), w(t))$ of (1) and (2) is not completely understood because the number of limit cycles is still unclear (for instance, [5], [6], [8], [17], [19]). We therefore rely on numerical methods to solve (1) and (2).

Let us specify the parameters in (1) as

$$r_1 = 576, \qquad r_2 = \frac{23616}{11}, \qquad r_3 = \frac{39456}{11}, \tag{6a}$$

$$a_1 = 572, \qquad a_2 = 1804, \qquad a_3 = 594, \tag{6b}$$

$$b_{12} = 308, \qquad b_{13} = 308, \qquad b_{21} = 4420, \tag{6c}$$

$$b_{23} = 308, \qquad b_{31} = 5850, \qquad b_{32} = 2970, \tag{6d}$$

which satisfy (A1)–(A4). Numerical simulation of (1) with (6) and (2) demonstrates the following: if w_0 is relatively small, $w(t)$ immediately fades out so that the solution $(u(t), v(t), w(t))$ tends to $\left(\frac{r_1}{a_1}, 0, 0\right) = (1.007\ldots, 0, 0)$; that is, U and V do not coexist (Figure 1(a)), but if w_0 is relatively large, $(u(t), v(t), w(t))$ tends to $(u^*, v^*, w^*) = (0.014\ldots, 1.014\ldots, 0.830\ldots)$ (Figure 1(b)). Consequently, (1) with (6) is a bistable system, in the sense that any solution generically tends to either $\left(\frac{r_1}{a_1}, 0, 0\right)$ or (u^*, v^*, w^*), as shown in Figure 2. This indicates that U and V coexist, depending on the initial value w_0.

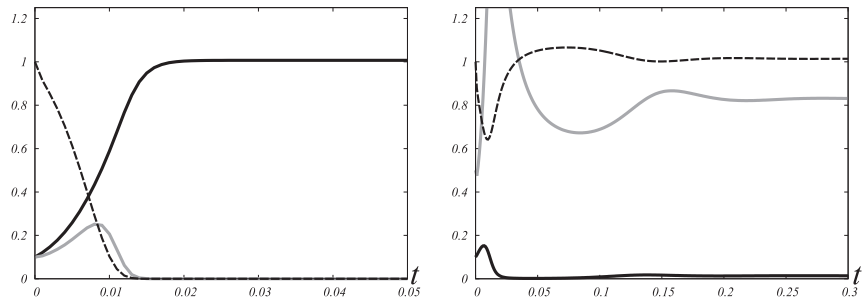

(a) $(u_0, v_0, w_0) = (0.1, 1.0, 0.1)$ (b) $(u_0, v_0, w_0) = (0.1, 1.0, 0.5)$

Fig. 1. Numerical simulation of (1) with (6) and (2) where u, v and w are indicated by the solid, dashed and grey solid lines, respectively.

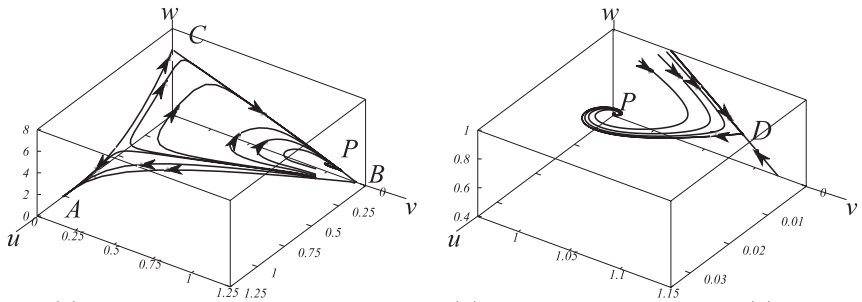

(a) Overall view of trajectories of (1) in (u, v, w)-space.

(b) Enlarged trajectories of (1) near P

Fig. 2. Bistable trajectories of (1) with (6) and (2) in (u, v, w)-space where $A = \left(\frac{r_1}{a_1}, 0, 0\right)$, $B = \left(0, \frac{r_2}{a_2}, 0\right)$, $C = \left(0, 0, \frac{r_3}{a_3}\right)$, $D = (0, \hat{v}, \hat{w})$ and $P = (u^*, v^*, w^*)$.

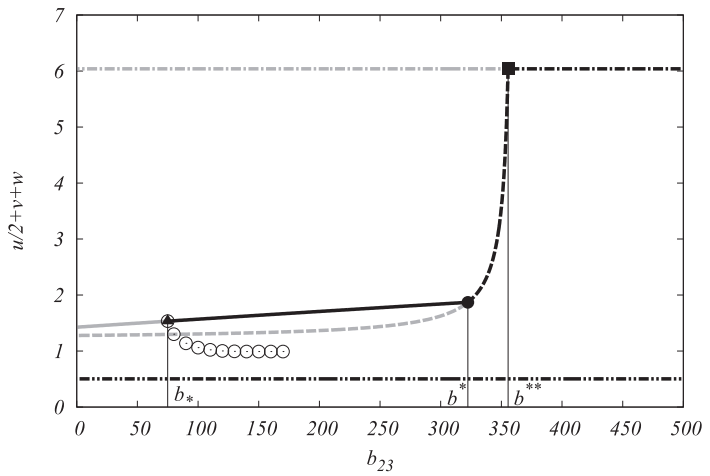

Fig. 3. Global structure of non-negative equilibrium points of (1). The dash-two dot line and the dash-one dot line represent $\left(\frac{r_1}{a_1}, 0, 0\right)$ and $\left(0, 0, \frac{r_3}{a_3}\right)$, respectively, which are independent of b_{23}. The dashed line and the solid line represent $(0, \hat{v}, \hat{w})$ and (u^*, v^*, w^*), respectively. ○ is the unstable limit cycle. Black and gray colors indicate stable and unstable solutions, ■ and ● indicate the stationary bifurcation points and ▲ indicates the Hopf bifurcation point. $(\check{u}, 0, \check{w})$ and $\left(0, \frac{r_2}{a_2}, 0\right)$ are not drawn in this figure, because they are unstable and not connected with any stable branch.

Thus far, we fixed $b_{23} = 308$ in Figures 1 and 2. We next take b_{23} as a free parameter, leaving other parameters fixed to satisfy (6) and draw the global structure of equilibrium points of (1) where b_{23} is globally varied in the interval $0 < b_{23} < 500$, as shown in Figure 3. We first note that $\left(\frac{r_1}{a_1}, 0, 0\right)$ ($-\cdots-$ in Figure 3) is stable and $\left(0, \frac{r_2}{a_2}, 0\right)$ is unstable for any b_{23}, whereas $\left(0, 0, \frac{r_3}{a_3}\right)$ ($-\cdot-$ in Figure 3) is stable for large b_{23}. When b_{23} decreases, $\left(0, 0, \frac{r_3}{a_3}\right)$

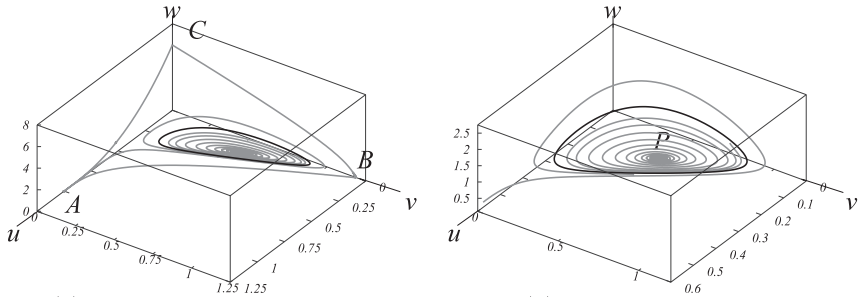

(a) Overall view of trajectories of the orbit in (u, v, w)-space.

(b) Enlarged trajectories of the orbit near P

Fig. 4. Unstable limit cycle of (1) at $b_{23} = 100$ in (u, v, w)-space, where $A = \left(\frac{r_1}{a_1}, 0, 0\right)$, $B = \left(0, \frac{r_2}{a_2}, 0\right)$, $C = \left(0, 0, \frac{r_3}{a_3}\right)$ and $P = (u^*, v^*, w^*)$. Black and gray lines are an unstable limit cycle and trajectories generically tending to either A or P, respectively.

is destabilized at $b_{23} = b^{**} = 355.53\ldots$ and $(0, \hat{v}, \hat{w})$ (– – – – in Figure 3) appears (■ in Figure 3). It bifurcates supercritically from $\left(0, 0, \frac{r_3}{a_3}\right)$ so that it is stable. When b_{23} still decreases, $(0, \hat{v}, \hat{w})$ is destablized at $b_{23} = b^* = 322.39\ldots$ and a positive equilibrium point (u^*, v^*, w^*) (——— in Figure 3) appears (● in Figure 3). It bifurcates supercritically from $(0, \hat{v}, \hat{w})$ so that it is stable. When b_{23} decreases even further, (u^*, v^*, w^*) is destablized through Hopf bifurcation at $b_{23} = b_* = 74.91\ldots$ (▲ in Figure 3), where an unstable limit cycle bifurcates subcritically from (u^*, v^*, w^*) when b_{23} increases (Figure 4). This limit cycle tends to a heteroclinic cycle with $(\check{u}, 0, \check{w}) \to \left(0, 0, \frac{r_3}{a_3}\right) \to (0, \hat{v}, \hat{w}) \to (\check{u}, 0, \check{w})$, as b_{23} increases to $174.42\ldots$.

Integrating the above, we find that the unique positive equilibrium solution (u^*, v^*, w^*) is stable for $b_* < b_{23} < b^*$. This condition on b_{23} is required for (A2) to hold.

Keeping this situation, we consider the case where the three competing species U, V and W move by diffusion and propose the following one-dimensional competition-diffusion system for $u(t, x)$, $v(t, x)$ and $w(t, x)$, which are respectively the population densities of U, V and W for time t and position x in $\mathbf{R}$:

$$\begin{cases} u_t = d_1 u_{xx} + (r_1 - a_1 u - b_{12} v - b_{13} w)u, \\ v_t = d_2 v_{xx} + (r_2 - b_{21} u - a_2 v - b_{23} w)v, \qquad t > 0,\ x \in \mathbf{R}, \\ w_t = d_3 w_{xx} + (r_3 - b_{31} u - b_{32} v - a_3 w)w, \end{cases} \tag{7}$$

where d_i $(i = 1, 2, 3)$ are the diffusion rates, which are positive constants, and r_i, a_i and b_{ij} $(i, j = 1, 2, 3\ (i \neq j))$ satisfy (A1)–(A4). For (7), we take the initial conditions

$$u(0, x) = u_0(x) \geq 0, \quad v(0, x) = v_0(x) \geq 0, \quad w(0, x) = w_0(x) \geq 0, \qquad x \in \mathbf{R}. \tag{8}$$

Then, the following questions arise: When W invades *locally* (in space) into the (U, V) system, does competitor-mediated coexistence occur for U and V? If so, does the coexistence of U and V exhibit either spatially constant or non-constant equilibrium? These questions motivate us to study whether there exist *stable spatially nonconstant* equilibrium solutions $(u(x), v(x), w(x))$ of (7). We first note that by the concept of Turing's diffusion-induced instability ([16]), local bifurcation theory can be applied to determining the existence of non-constant equilibrium solutions with small amplitudes which bifurcate from the spatially constant equilibrium solution (u^*, v^*, w^*) when some diffusion rates are suitably changed ([13]).

In this paper, we are concerned with existence and stability of non-constant equilibrium solutions with large amplitudes, which are shown in Figures 9 and 10. Our strategy is to use two procedures complementarily: one is a numerical tracking procedure of drawing the global structure of equilibrium solutions and the other is a semi-exact representation for finding non-constant equilibrium solutions.

To begin with, we consider the problem

$$\begin{cases} u_t = d_1 u_{xx} + (r_1 - a_1 u - b_{13} w)u, \\ w_t = d_3 w_{xx} + (r_3 - b_{31} u - a_3 w)w. \end{cases} \qquad t > 0,\ x \in \mathbf{R}, \tag{9}$$

with the boundary conditions

$$\begin{cases} \lim\limits_{x \to -\infty} (u(t,x), w(t,x)) = \left(\dfrac{r_1}{a_1}, 0\right), \\ \lim\limits_{x \to \infty} (u(t,x), w(t,x)) = \left(0, \dfrac{r_3}{a_3}\right). \end{cases} \qquad t > 0, \tag{10}$$

(A3) indicates that (9) and (10) possesses a stable travelling front solution $(u(x - ct), w(x - ct))$ (with unique velocity c [11]). If the velocity c is positive, U is stronger than W in spatial competition. Combining this with (A1) where U is absolutely stronger than V, we can say that U is the strongest among U, V and W. Therefore we may expect that only U survives after large time, that is, the competitor-mediated coexistence does not occur. For this reason, we assume the following:

(A5) the travelling velocity c is negative,

which indicates that in the absence of V, W is stronger than U in terms of the spatial competition.

2. Numerical simulations

In this section, we numerically study (7) and (8) in $\mathbf{R}$, with the boundary conditions

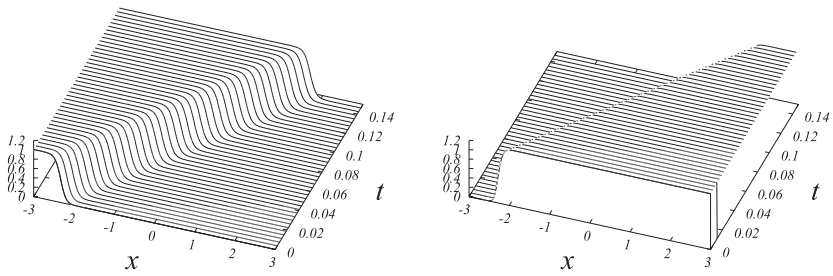

(a) u (b) v

Fig. 5. Numerical simulation of (13)–(15) where d_i, r_i, a_i, and b_{ij} $(i, j = 1, 2\ (i \neq j))$ satisfy (12) and (6).

$$\begin{cases} \lim_{x\to-\infty}(u(t,x), v(t,x), w(t,x)) = \left(\dfrac{r_1}{a_1}, 0, 0\right), \\ \lim_{x\to\infty}(u(t,x), v(t,x), w(t,x)) = \left(0, \dfrac{r_2}{a_2}, 0\right). \end{cases} \qquad t > 0, \tag{11}$$

Here we assume that the parameters in (7) satisfy (6) and

$$d_1 = d_2 = d_3 = 1. \tag{12}$$

We first consider the problem (7), (8) and (11) in the absence of w. That is,

$$\begin{cases} u_t = u_{xx} + (r_1 - a_1 u - b_{12} v)u, \\ v_t = v_{xx} + (r_2 - b_{21} u - a_2 v)v, \end{cases} \qquad t > 0,\ x \in \mathbf{R}, \tag{13}$$

with

$$u(0,x) = u_0(x), \quad v(0,x) = v_0(x) \qquad x \in \mathbf{R}, \tag{14}$$

where

$$\begin{cases} \lim_{x\to-\infty}(u_0(x), v_0(x)) = \left(\dfrac{r_1}{a_1}, 0\right), \\ \lim_{x\to\infty}(u_0(x), v_0(x)) = \left(0, \dfrac{r_2}{a_2}\right). \end{cases} \tag{15}$$

Then, as shown in Figure 5, the solution $(u(t,x), v(t,x))$ behaves as if it were a travelling front with constant velocity and constant shape, which propagates towards the right. This behavior is easily expected from (A1).

We now consider the situation where W invades the (U, V) system. That is, we take the initial conditions (8) as

$$u(0,x) = u(t_0,x), \quad v(0,x) = v(t_0,x), \quad w(0,x) = w_0(x) \geq 0, \qquad x \in \mathbf{R}, \tag{16}$$

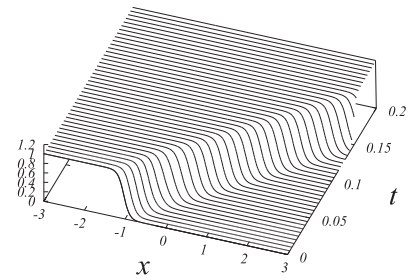

(a) u

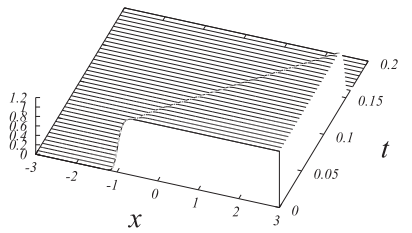

(b) v

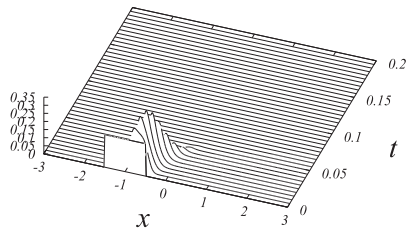

(c) w

Fig. 6. Numerical simulation of (7), (11) and (16) where d_i, r_i, a_i, and b_{ij} $(i, j = 1, 2, 3\ (i \neq j))$ satisfy (12) and (6). $w_0(x)$ is relatively small (width is 1.0 and height is 0.1).

where $(u(t_0, x), v(t_0, x))$ is a solution of (13)–(15) for suitably fixed t_0, and $w_0(x)$ is taken in some overlapped zone of $u(t_0, x)$ and $v(t_0, x)$. We consider (7), (11) and (16). If $w_0(x)$ is relatively small, $w(t, x)$ immediately fades out so that u still propagates towards the right and becomes dominant in space, as shown in Figure 6.

On the contrary, if $w_0(x)$ is relatively large, the resulting behavior is different: w persists, $(u(t, x), v(t, x), w(t, x))$ propagates in both directions and (u^*, v^*, w^*) becomes dominant in space, as shown in Figures 7 and 8. Moreover, Figures 8 (g) and (h) suggest the appearance of a travelling wave solution satisfying

$$\begin{cases} \lim\limits_{x \to -\infty} (u(t, x), v(t, x), w(t, x)) = (u^*, v^*, w^*), \\ \lim\limits_{x \to \infty} (u(t, x), v(t, x), w(t, x)) = \left(\frac{r_1}{a_1}, 0, 0\right), \end{cases} \tag{17}$$

which propagates towards the right.

If w_0 is at suitably medium value, the situation is drastically different. As shown in Figures 9 and 10, u and v can coexist locally in space. After a large

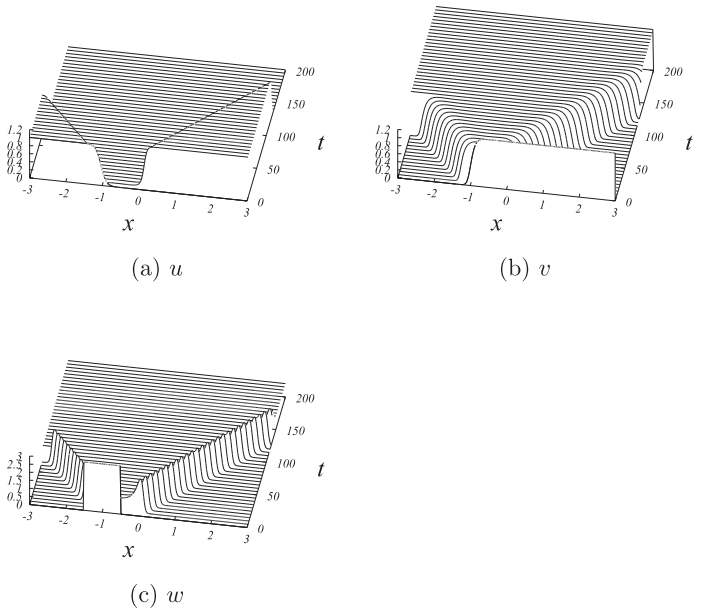

Fig. 7. Numerical simulation of (7), (11) and (16) where d_i, r_i, a_i, and b_{ij} $(i, j = 1, 2, 3\ (i \neq j))$ satisfy (12) and (6). $w_0(x)$ is relatively large (width is 1.0 and height is 3.0).

period of time, the solution decomposes into two dynamics: one is a travelling wave of u, v and $w \equiv 0$, satisfying (11) which propagates towards the right, and the other is a non-constant, spatially symmetric standing wave of u, v and w, satisfying

$$\lim_{|x|\to\infty} (u(t,x), v(t,x), w(t,x)) = \left(\frac{r_1}{a_1}, 0, 0\right). \tag{18}$$

Consequently, when the parameters are specified to satisfy (6), numerical simulation suggests the existence of a *stable* non-constant equilibrium solution $(u(x), v(x), w(x))$, where the profile of $w(x)$ exhibits two humps as shown in Figure 10 (f).

3. Global structure of equilibrium solutions

In this section, motivated by Figure 10 (f), we study the non-constant equilibrium solutions of (7) and (18). By (A5) in Section 2, we first note that there exists an unstable non-constant equilibrium solution (say $(\bar{u}(x), \bar{w}(x))$) of (9) with the boundary conditions

$$\lim_{|x|\to\infty} (u(t,x), w(t,x)) = \left(\frac{r_1}{a_1}, 0\right), \tag{19}$$

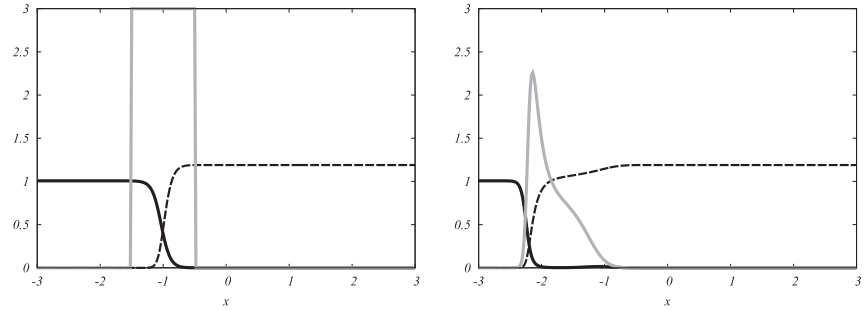

(a) $t = 0$ (b) $t = 0.04$

(c) $t = 0.06$ (d) $t = 0.10$

(e) $t = 0.50$ (f) $t = 50.0$

(g) $t = 100.$ (h) $t = 200.$

Fig. 8. Snapshots of (u, v, w) in Figure 7 where u, v and w are represented by the solid line, dotted line and grey solid line, respectively.

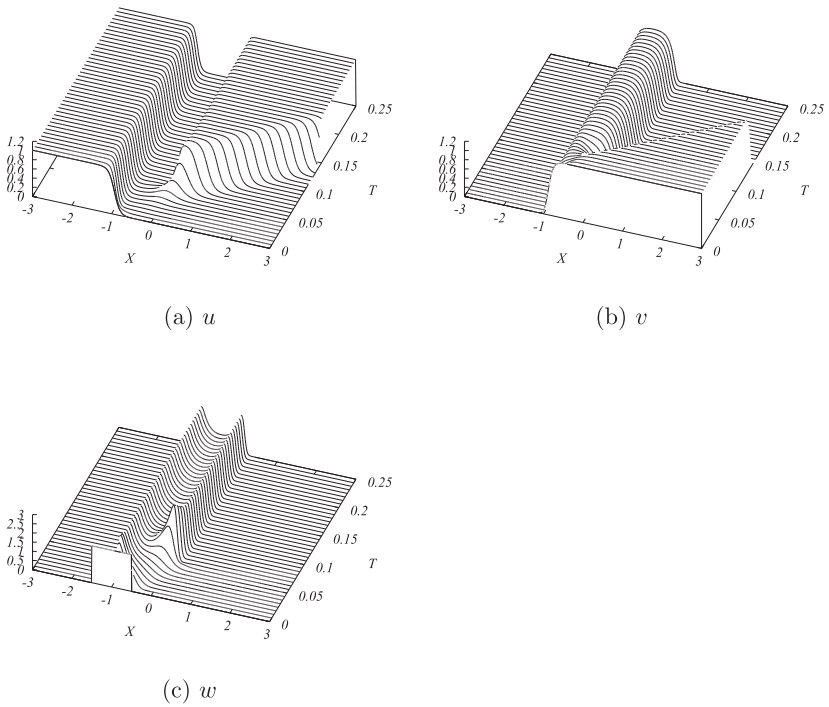

(a) u (b) v

(c) w

Fig. 9. Numerical simulation of (7), (11) and (16) where d_i, r_i, a_i, and b_{ij} $(i, j = 1, 2, 3\ (i \neq j))$ satisfy (12) and (6). $w_0(x)$ is relatively medium (width is 1.0 and height is 2.0).

as shown in Figure 11 ([9], [10] and [11]). This implies that $(\bar{u}(x), 0, \bar{w}(x))$ is an unstable trivial non-constant equilibrium solution of (7) and (18) for any b_{23}.

By using AUTO ([3]), we numerically plotted the global structure of spatially non-constant equilibrium solutions of (7) and (18) for various b_{23} leaving other parameters fixed to satisfy (6) and (12). From this structure, shown in Figure 12, several conclusions can be drawn regarding the non-constant equilibrium solutions.

(1) The unstable trivial branch of $(\bar{u}(x), 0, \bar{w}(x))$ (say B_0) exists for any b_{23}. When b_{23} increases, a nontrivial branch of $(u^{**}(x), v^{**}(x), w^{**}(x))$ (say B_1) is bifurcated from B_0 at BP $(b_{23} = b_{BP}(= 110.63\ldots))$ where $v(x) \geq 0$ but is not identically zero. This nontrivial branch B_1 is still unstable.

(2) As b_{23} increases, the unstable nontrivial branch B_1 becomes stable through Hopf bifurcation at HB $(b_{23} = b_{HB}(= 223.09\ldots))$ so that it is stable for $b_{23} > b_{HB}$.

(3) Along the stable branch B_1, there occurs a saddle node bifurcation at SN $(b_{23} = b_{SN}(= 308.04\ldots))$ so that it loses stability at $b_{23} = b_{SN}$ and an unstable branch B_2 exists for $b_{LIMIT}(= 307.97\ldots) < b_{23} <$

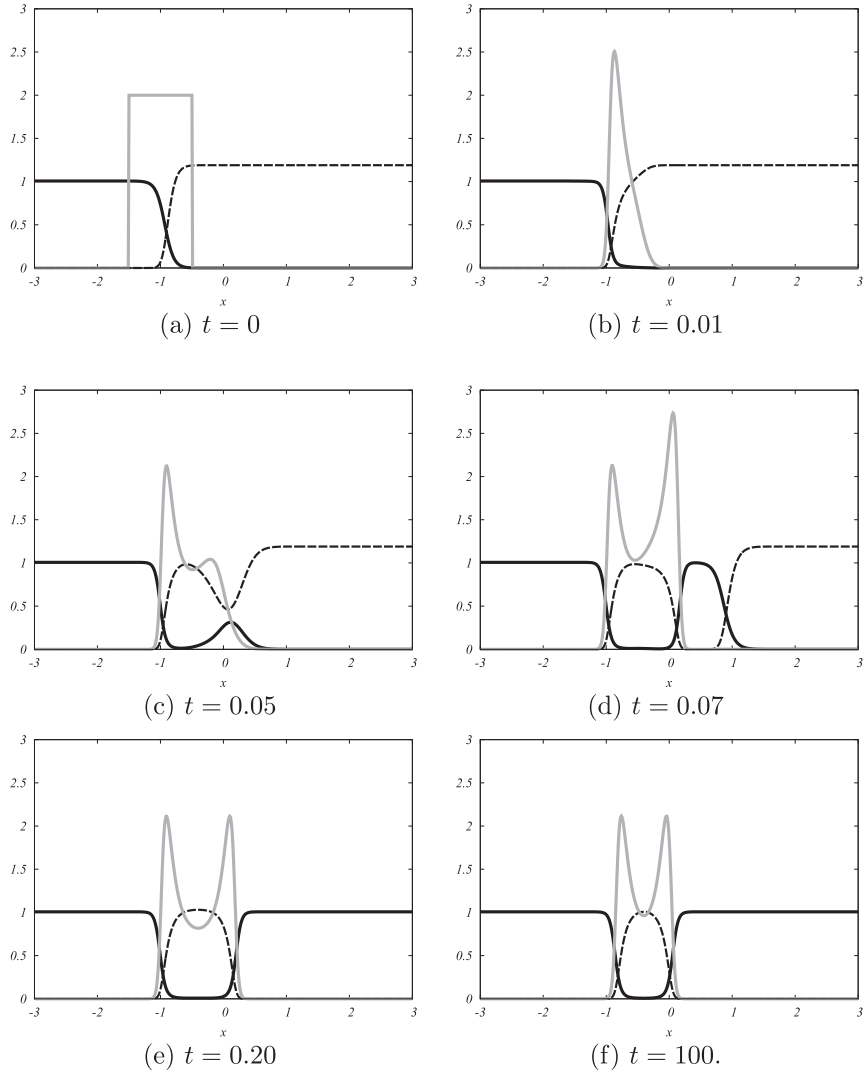

Fig. 10. Snapshots of (u, v, w) in Figure 9 where u, v and w are drawn by a solid line, a dotted line and a grey solid line, respectively.

b_{SN}, so that there coexist two nontrivial equilibrium branches B_1 and B_2 where the lower branch B_1 is stable, whereas the upper branch B_2 is unstable.

(4) For $b_{23} > b_{SN}$, there is no nontrivial branch.

The global structure in Figure 12 indicates that for b_{23} satisfying $b_{LIMIT} < b_{23} < b_{SN}$, (7) and (18) possess **(a)** a stable trivial constant equilibrium

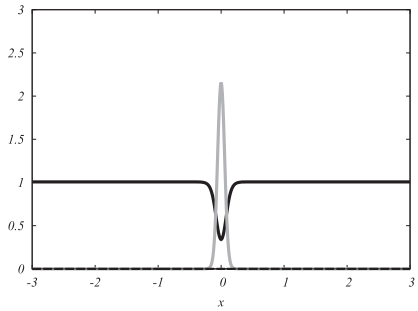

Fig. 11. The unstable trivial non-constant equilibrium solution $(\bar{u}(x), \bar{w}(x))$ of (9) with (19), where $\bar{u}$ and $\bar{w}$ are drawn by a solid line and a gray line, respectively.

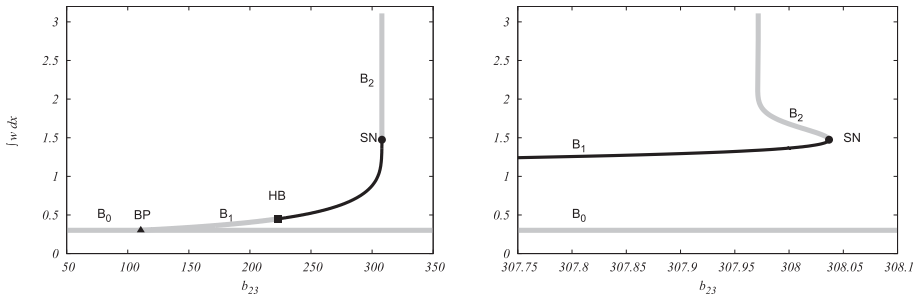

(a) Overall view of bifurcation diagram of equilibrium solutions of (7) with (18).

(b) Enlarged bifurcation diagram shown in (a)

Fig. 12. Bifurcation diagram of spatially non-constant equilibrium solutions of (7) and (18). The solid (resp. gray solid) line represents the stable (resp. unstable) equilibrium branches. The parameters are fixed to satisfy (6) and (12) except for b_{23}. B_0 indicates the trivial branch consisting of $(\bar{u}(x), 0, \bar{w}(x))$ where $(\bar{u}(x), \bar{w}(x))$ is shown in Figure 11. B_1 and B_2 indicate a nontrivial branch where $v(x) \geq 0$ but is not identically zero. *BP* ($b_{23} = b_{BP} = 110.65\ldots$), *HB* ($b_{23} = b_{HB} = 223.09\ldots$) and *SN* ($b_{23} = b_{SN} = 308.04\ldots$) indicate the stationary bifurcation point on which B_1 bifurcates from B_0, the Hopf bifurcation point at which B_1 recovers its stability, and the saddle node point at which B_1 loses its stability, respectively.

$\left(\frac{r_1}{a_1}, 0, 0\right)$, **(b)** an unstable trivial non-constant equilibrium $(\bar{u}(x), 0, \bar{w}(x))$, **(c)** a stable nontrivial non-constant equilibrium, and **(d)** an unstable nontrivial non-constant equilibrium. When the parameters satisfy (6), the equilibrium solutions (a)–(d) are as shown in Figures 13 (a)–(d).

Our next problem is to show the existence of the stable nontrivial non-constant equilibrium solution (c), which indicates the competitor-mediated coexistence of U and V. The standard approach is to begin with the sixth-order autonomous ODEs derived from (7) to obtain non-constant solutions

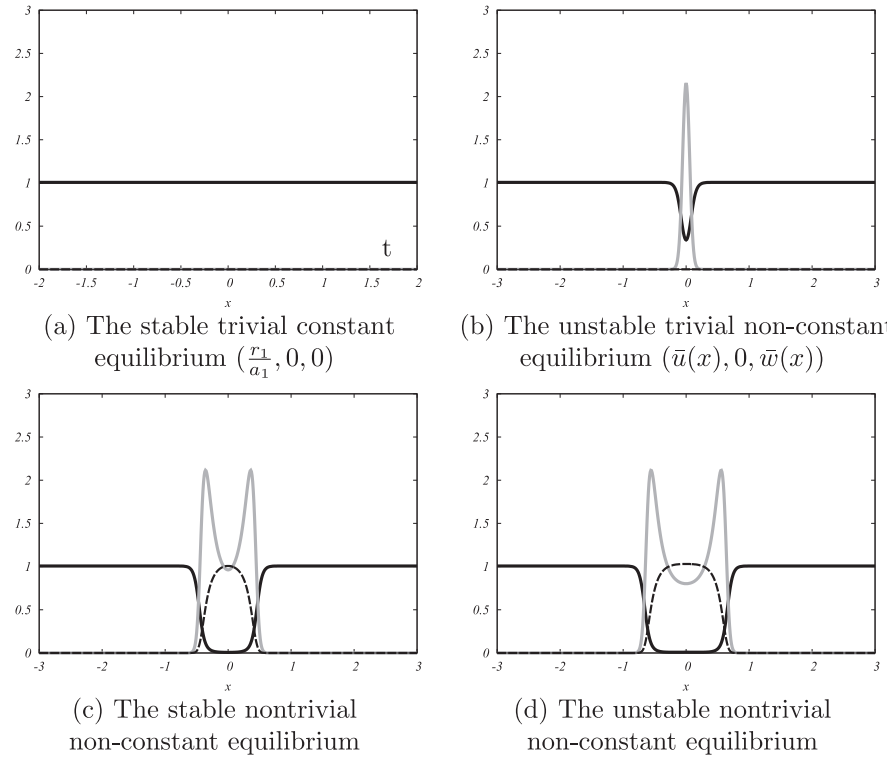

(a) The stable trivial constant equilibrium $(\frac{r_1}{a_1}, 0, 0)$

(b) The unstable trivial non-constant equilibrium $(\bar{u}(x), 0, \bar{w}(x))$

(c) The stable nontrivial non-constant equilibrium

(d) The unstable nontrivial non-constant equilibrium

Fig. 13. Spatial profiles of constant and non-constant equilibrium solutions of (7) and (18), where u, v and w are represented by the solid line, dotted line and grey solid line, respectively. The parameters are specified to satisfy (6) and (12).

(c). However, this is quite difficult because the solutions exhibit strong inhomogeneity, as shown in Figures 13 (c) and (d). Therefore, we instead pursue an alternative approach: we apply a new approach which generalizes the method of finding exact travelling wave solutions developed in [2] and obtain semi-exact standing wave (equilibrium) solutions of (7) and (18). This is described in the next section.

4. Semi-exact representation of equilibrium solutions

In this section, we consider the following stationary problem:

$$\begin{cases} 0 = d_1 u_{xx} + (r_1 - a_1 u - b_{12} v - b_{13} w)u, \\ 0 = d_2 v_{xx} + (r_2 - b_{21} u - a_2 v - b_{23} w)v, \qquad x \in \mathbf{R}, \\ 0 = d_3 w_{xx} + (r_3 - b_{31} u - b_{32} v - a_3 w)w. \end{cases} \tag{20}$$

with the boundary conditions

$$\lim_{|x|\to\infty}(u,v,w)(x)=\left(\frac{r_1}{a_1},0,0\right). \tag{21}$$

As mentioned above, $(u,v,w)(x)\equiv\left(\frac{r_1}{a_1},0,0\right)$ and $(\bar{u}(x),0,\bar{w}(x))$ are trivial solutions of (20) and (21) (Figures 13 (a) and (b)). Our goal is to seek nontrivial solutions with profiles similar to (c) and (d) in Figure 13. Our new approach, which is basically developed in [2], finds exact travelling wave solutions of (7) under a different situation from the present one.

As a scalar version of (1), we have the Fisher–KPP equation

$$u_t=du_{xx}+(r-au)u, \tag{22}$$

for which it is well known that some travelling wave solution can be formulated explicitly in terms of tanh function ([1]). For systems of two equations, Rodrigo and Mimura ([14] and [15]) developed a systematic method to find exact travelling wave solutions. In their result, the tanh function again plays a key role in many cases. In the previous paper [2], an attempt was made to generalize Rodrigo and Mimura's method to find exact travelling wave solutions of system (7). Unfortunately, due to the high complexity of a system of three equations, there seems to be no simple systematic analytical method as in the two-equation cases to find exact solutions of (7). However, from the examples of exact solutions obtained for one equation and two equations, we make the following observations:

(P1) $\dfrac{d\tanh x}{dx}=1-\tanh^2 x$; that is, the derivative of tanh is a simple polynomial of tanh;

(P2) It seems natural to assume that u, v and w are quadratic polynomials of tanh.

From (P1) and (P2), very interesting exact travelling solutions of (7) were obtained [2] with the help of the software MATHEMATICA ([18]). To apply this approach to find solutions similar to (c) and (d) in Figure 13, we assumed that u, v and w are polynomials of tanh with degree greater than two in order to have more complicated profiles. Unfortunately, we failed to find any exact solution similar to (c) or (d) in Figure 13 under this assumption. Therefore, it is natural to think that the exact solutions should be expressed in terms of some function $T(x)$ other than tanh. To mimic (P1) and (P2), we make two assumptions as follows:

(H1) $T(x)\to -1$ as $x\to-\infty$ and $T(x)\to 1$ as $x\to\infty$. $\dfrac{dT(x)}{dx}$ is a simple polynomial of $T(x)$ containing the factor $1-T^2(x)$.

(H2) u, v, and w are simple polynomials of $T(x)$.

In (H1), we must assume $\dfrac{dT(x)}{dx}$ contains the factor $1-T^2(x)$ so that $\frac{dT(x)}{dx}\to 0$ as $|x|\to\infty$. If the degrees of the polynomials in (H1) and (H2) are high, we have on the one hand more free coefficients, but on the other hand, more algebraic conditions to satisfy when the relations in (H1) and (H2) are put in (20). To keep the numbers of free coefficients and algebraic restrictions balanced, it is better to set some of the degrees of the polynomials in (H1) and (H2) to values greater than 2 but not too large.

Following this idea, with the help of the software MATHEMATICA, we can obtain two types of solutions with a family of parameter n for the problem represented by (20) and (21), for which the following two conditions on the parameters in (20) are assumed, respectively:

$$\begin{cases} d_1=d_2=d_3=1, \\ r_1=4(2+n)^2,\ r_2=\frac{4(2+n)^2(16+11n)}{1+n},\ r_3=\frac{4(2+n)^2(21+16n)}{1+n}, \\ a_1=4(1+n)(2+n),\ b_{12}=4n(1+n),\ b_{13}=10(1+n)^2, \\ b_{21}=20(2+n)(4+3n),\ a_2=4(1+n)(16+11n),\ b_{23}=28(1+n)^2, \\ b_{31}=20(2+n)(5+4n),\ b_{32}=16(1+n)(5+4n),\ a_3=54(1+n)^2, \end{cases} \tag{23}$$

and

$$\begin{cases} d_1=d_2=d_3=1, \\ r_1=4(2+n)^2,\ r_2=\frac{2(2+n)^2(12+7n)}{1+n},\ r_3=\frac{2(2+n)^2(17+12n)}{1+n}, \\ a_1=4(1+n)(3+n),\ b_{12}=4(-3+n)(1+n),\ b_{13}=28(1+n), \\ b_{21}=10(3+n)(4+3n),\ a_2=2(1+n)(12+7n),\ b_{23}=28(1+n), \\ b_{31}=10(3+n)(5+4n),\ b_{32}=6(1+n)(5+4n),\ a_3=54(1+n). \end{cases} \tag{24}$$

In the formulas (23) and (24), we have a free parameter n which is constant. We are now in a position to give type-I and type-II solutions of (20) and (21) as follows:

THEOREM 1 (Type-I solution). *Assume that* (23) *with a free parameter* $n>0$ *is satisfied. Then the problem represented by* (20) *and* (21) *admits a solution of the form*

$$\begin{cases} u(x)=\dfrac{1}{1+n}[1+(1+n)T^2(x)], \\ v(x)=[1-T^2(x)]^2, \\ w(x)=\dfrac{1}{1+n}[1+(1+n)T^2(x)][1-T^2(x)]^2, \end{cases} \tag{25}$$

where $T = T(x)$ *is the solution of the following problem*

$$\begin{cases} \dfrac{d}{dx}T(x) = [1 - T^2(x)][1 + (1+n)T^2(x)], \quad x \in \mathbf{R}, \\ T(0) = 0. \end{cases} \tag{26}$$

We note that the solution of (26) can be obtained implicitly to give

$$\frac{1}{2n+4}\ln\left[\frac{1+T(x)}{1-T(x)}\right] + \frac{\sqrt{n+1}}{n+2}\tan^{-1}[\sqrt{n+1}T(x)] = x. \tag{27}$$

If $T(x)$ of (26) or (27) is solved numerically, the profile of the solution $(u(x), v(x), w(x))$ of (20) and (21) can be explicitly given; Figure 14 shows some examples. This procedure is therefore called the semi-exact representation of the solution of (20) and (21).

THEOREM 2 (Type-II solution). *Suppose that* (24) *is satisfied for any* $n > 3$. *Then the problem represented by* (20) *and* (21) *admits a solution of the form*

$$\begin{cases} u(x) = \dfrac{1}{(1+n)(3+n)}[1 + (1+n)T^2(x)]^2, \\ v(x) = [1 - T^2(x)]^2, \\ w(x) = [1 + (1+n)T^2(x)][1 - T^2(x)]^2, \end{cases} \tag{28}$$

where $T = T(x)$ *is the solution of* (26) *or* (27).

Figure 15 shows some examples of type-II solutions. We remark that when $n = 10$ in (24), the parameters are identical to those in (6) and (12). This indicates that the stable non-trivial non-constant equilibrium solution numerically obtained in Figure 13 (c) is given by the semi-exact equilibrium solution of type-II (see Figures 13 (c) and 15 (d)).

Both Theorems 1 and 2 can be verified in MATHEMATICA directly. However, without knowing the relations (23)–(26) and (28) in advance, it is difficult to find them since the computation is quite involved. The requisite formulas (23)–(26) and (28) can be obtained as follows: First assume $T(x)$ has a particular form, e.g. the one in (26), and n is assigned a particular prime number, say 7. If the computation is not impractically complex and some exact solutions can be found, together with suitable coefficients in the nonlinear terms of (20), then we change to another prime number n to find corresponding exact solutions and coefficients. We repeat this procedure several times. In

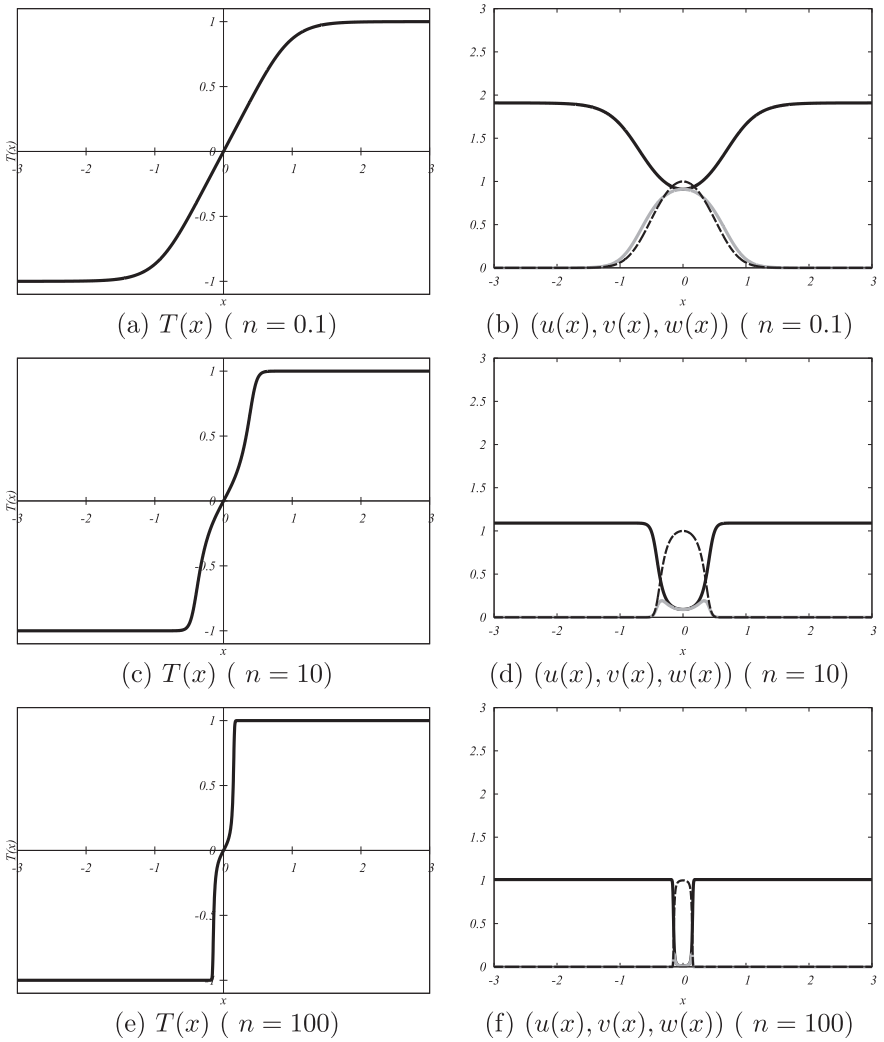

Fig. 14. $T(x)$ and semi-exact solutions of one hump $(u(x), v(x), w(x))$ of Type-I where u, v and w are represented by the solid line, dashed line and grey solid line, respectively.

each iteration, the coefficients in (20) obtained are factorized into prime factors. We observe how the prime factors in these coefficients change according to different prime n and determine that the linear factors $n+1$, $5+4n$, $16+11n$, etc., should appear in (23)–(25) and (28). This procedure affords general formulas of exact solutions with parameter n.

It is interesting to note that type-I solutions satisfy the special relation $w = uv$, whereas type-II solutions satisfy $w = \sqrt{(n+1)(n+3)}\sqrt{u}v$. In the

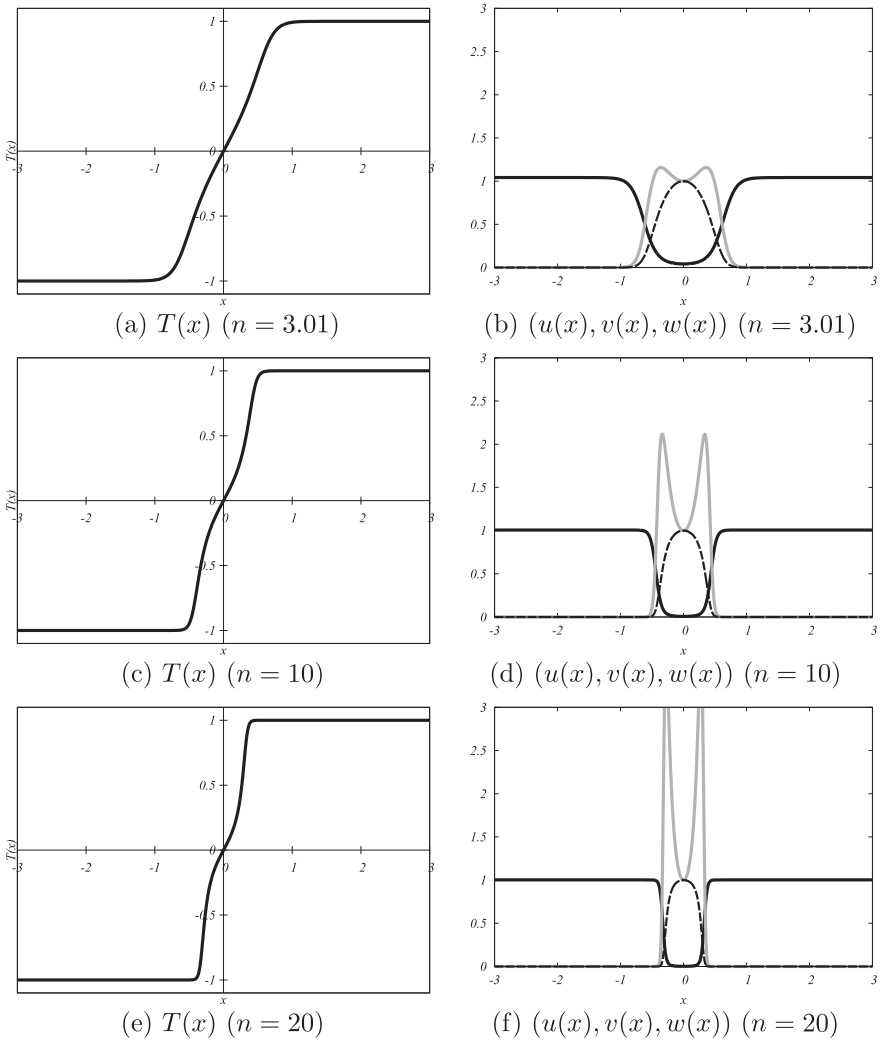

(a) $T(x)$ $(n = 3.01)$ (b) $(u(x), v(x), w(x))$ $(n = 3.01)$

(c) $T(x)$ $(n = 10)$ (d) $(u(x), v(x), w(x))$ $(n = 10)$

(e) $T(x)$ $(n = 20)$ (f) $(u(x), v(x), w(x))$ $(n = 20)$

Fig. 15. $T(x)$ and semi-exact solutions of two humps $(u(x), v(x), w(x))$ of Type-II where u, v and w are represented by the solid line, dashed line and grey solid line, respectively.

appendix, we show more generalized versions of the semi-exact representation of non-constant equilibrium solutions.

The formulas for type-I and type-II solutions reveal very interesting phenomena when the parameter n tends to ∞. Let σ_- and σ_+ satisfy $T(\sigma_\pm) = \pm 1/2$. We consider the scaling $z = nx$, $U_n(z) = u(z/n + \sigma)$, $V_n(z) = v(z/n + \sigma)$, $W_n(z) = w(z/n + \sigma)$ and $S_n(z) = T(x/n + \sigma)$, where σ will be taken as σ_- or σ_+. Let $U(z)$, $V(z)$, $W(z)$ and $S(z)$ denote the limits of $U_n(z)$, $V_n(z)$, $W_n(z)$

and $S_n(z)$ as $n \to \infty$ respectively. Then for type-I solution, as $n \to \infty$, the limit of (20) divided by n^2 converges to the following system, which constitutes the limit equations for U, V and W,

$$\begin{cases} 0 = d_1 U_{zz} + (4 - 4U - 4V - 10W)U, \\ 0 = d_2 V_{zz} + (44 - 60U - 44V - 28W)V, \\ 0 = d_3 W_{zz} + (64 - 80U - 64V - 54W)W, \end{cases} \qquad x \in \mathbf{R} \tag{29}$$

with the boundary condition at $-\infty$

$$\lim_{z \to -\infty} (U, V, W)(x) = (1, 0, 0). \tag{30}$$

Moreover, $S(z)$ satisfies the equation

$$\begin{cases} \dfrac{d}{dz} S(z) = [1 - S^2(z)]S^2(Z), \quad z \in \mathbf{R}, \\ S(0) = \begin{cases} -\frac{1}{2} & \text{if } \sigma = \sigma_-; \\ \frac{1}{2} & \text{if } \sigma = \sigma_+. \end{cases} \end{cases} \tag{31}$$

Note that $\lim_{z \to -\infty} S(z) = -1$ and $\lim_{z \to \infty} S(z) = 0$ if $\sigma = \sigma_-$; $\lim_{z \to -\infty} S(z) = 0$, and $\lim_{z \to \infty} S(z) = 1$ if $\sigma = \sigma_+$. By ODE theory or standard elliptic estimates, one can show that $U_n(z)$, $V_n(z)$, $W_n(z)$ and $S_n(z)$ converge to $U(z)$, $V(z)$, $W(z)$ and $S(z)$, respectively, in C^2 on any compact set as $n \to \infty$.

Therefore we have the following theorem:

THEOREM 3 (One-hump solution—I). *Let $\sigma = \sigma_-$. The problem represented by* (29) *and* (30) *admits a solution of the form*

$$\begin{cases} U(z) = S^2(z), \\ V(z) = [1 - S^2(z)]^2, \\ W(x) = S^2(z)[1 - S^2(z)]^2, \end{cases} \tag{32}$$

where $S(z)$ is the solution of (31).

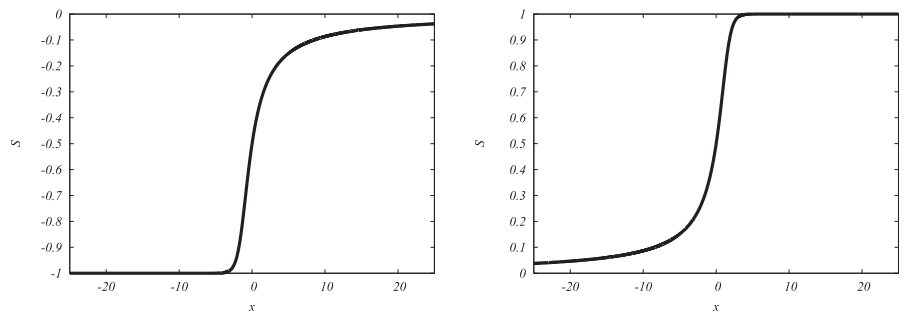

(a) $S(x)$ ($\sigma = \sigma_-$) (b) $S(x)$ ($\sigma = \sigma_+$)

Fig. 16. $S(x)$, the solution of (31)

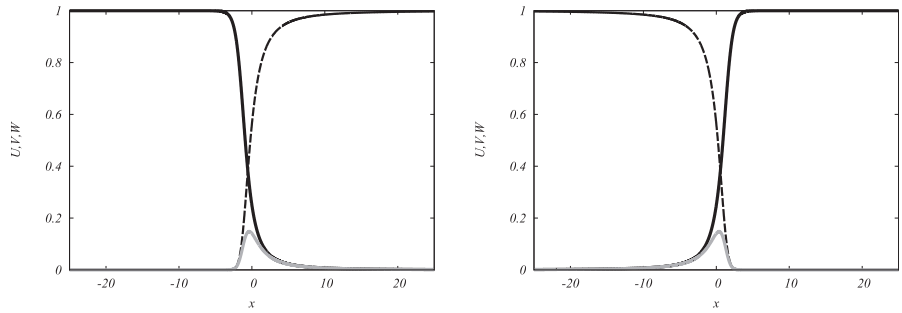

(a) $(u(x), v(x), w(x))$ for $\sigma = \sigma_-$ (b) $(u(x), v(x), w(x))$ for $\sigma = \sigma_+$

Fig. 17. One-hump solution $(u(x), v(x), w(x))$ of (29) and (30), where u, v and w are represented by the solid line, dashed line and grey solid line, respectively.

In [2], a one-hump travelling wave of three species is first constructed by using the tanh function. It is fascinating that through taking a limit of the two-hump solutions, the above theorem affords a one-hump solution that can be represented by the function $S(z)$, which differs from tanh. If we take $\sigma = \sigma_+$, another one-hump solution can be constructed which equals the solution in the above theorem with z replacing by $-z$.

For type-II solutions in (28), we take the same scaling as above except that we let $W_n(z) = 1/nw(z/n + \sigma)$. Then as $n \to \infty$, the limit of (20) divided by n^2 converges to the following system, which constitutes the equations for the limit functions U, V and W:

$$\begin{cases} 0 = d_1 U_{zz} + (4 - 4U - 4V - 28W)U, \\ 0 = d_2 V_{zz} + (14 - 30U - 14V - 28W)V, \\ 0 = d_3 W_{zz} + (24 - 40U - 24V - 54W)W, \end{cases} \qquad x \in \mathbf{R} \tag{33}$$

with the boundary condition at $-\infty$

$$\lim_{z \to -\infty} (U, V, W)(z) = (1, 0, 0). \tag{34}$$

We then have the following result:

THEOREM 4 (One-hump solution—II). *Let $\sigma = \sigma_-$. The problem* (33) *and* (34) *admits a solution of the form*

$$\begin{cases} U(z) = S^4(z), \\ V(z) = [1 - S^2(z)]^2, \\ W(x) = S^2(z)[1 - S^2(z)]^2, \end{cases} \tag{35}$$

where $S(z)$ is the solution of (31).

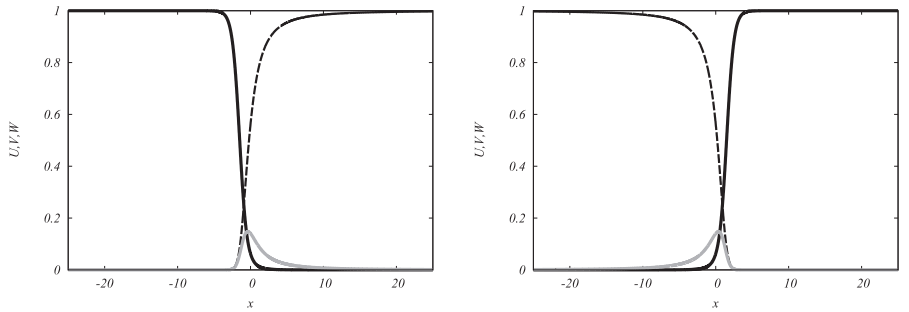

(a) $(u(x), v(x), w(x))$ for $\sigma = \sigma_-$ (b) $(u(x), v(x), w(x))$ for $\sigma = \sigma_+$

Fig. 18. One-hump solution $(u(x), v(x), w(x))$ of (33) and (34), where u, v and w are represented by the solid line, dashed line and grey solid line, respectively.

We can also employ scaling different from the above. We take $z = \sqrt{n}x$ instead of $z = nx$ and let $U_n(z) = u(z/\sqrt{n})$, $V_n(z) = v(z/\sqrt{n})$, $W_n(z) = w(z/\sqrt{n})$ and $S_n(z) = T(x/\sqrt{n})$. Let α_+ and α_- denote the unique positive root and unique negative root of

$$\frac{1}{2}\ln\left[\frac{1+\alpha}{1-\alpha}\right] - \frac{1}{\alpha} = 0 \tag{36}$$

respectively. Then from type-I solutions, we obtain the following theorem.

THEOREM 5 (Singular limit). *$U_n(z)$, $V_n(z)$, $W_n(z)$ and $S_n(z)$ converge to $U(z)$, $V(z)$, $W(z)$ and $S(z)$ pointwise as $n \to \infty$ respectively, where*

$$\begin{cases} U(z) = S^2(z), \\ V(z) = [1 - S^2(z)]^2, \\ W(x) = S^2(z)[1 - S^2(z)]^2, \end{cases} \tag{37}$$

and

$$S(z) = \begin{cases} -1 & \text{for } z < -\pi/2; \\ \alpha_- & \text{for } z = -\pi/2; \\ 0 & \text{for } -\pi/2 < z < \pi/2; \\ \alpha_+ & \text{for } z = \pi/2; \\ 1 & \text{for } z > \pi/2. \end{cases} \tag{38}$$

PROOF. By (26), $-1 < S_n(z) = T(x/\sqrt{n}) < 1$ and $S_n(z)$ is monotone. Therefore, $S_n(z) > 0$ for $z > 0$ and $S_n(z) < 0$ for $z < 0$. Let z be fixed. Assume that for some sequence $n_k \to \infty$, $\lim_{k\to\infty} S_{n_k}(z) = \alpha$ and $\lim_{k\to\infty} \sqrt{n_k + 1}S_{n_k}(z) = \beta$. Multiplying (27) by $\sqrt{n_k}$, we obtain

$$\frac{\sqrt{n_k}}{2n_k + 4}\ln\left[\frac{1 + S_{n_k}(z)}{1 - S_{n_k}(z)}\right] + \frac{\sqrt{n_k}\sqrt{n_k + 1}}{n_k + 2}\tan^{-1}[\sqrt{n_k + 1}S_{n_k}(z)] = z. \tag{39}$$

The two terms on the left-hand side of (39) have the same sign. Thus, we have

$$\frac{\sqrt{n_k}\sqrt{n_k+1}}{n_k+2}\tan^{-1}[\sqrt{n_k+1}S_{n_k}(z)] \le z \qquad \text{for } z \ge 0. \tag{40}$$

As $k \to \infty$, (40) becomes

$$\tan^{-1}[\beta] \le z \qquad \text{for } z \ge 0. \tag{41}$$

This implies

$$\alpha = 0, \qquad 0 \le \beta < \infty \text{ for } 0 \le z < \pi/2. \tag{42}$$

Therefore, we conclude that $S(z) = \lim_{n\to\infty} S_n(z)$ exists and equals 0 for $0 \le z < \pi/2$. By a similar argument, we can obtain $S(z) = \lim_{n\to\infty} S_n(z) = 0$ for $-\pi/2 < z \le 0$.

For $z = \pi/2$, we expand (39) in terms of n to obtain

$$\frac{1}{\sqrt{n_k}}\left\{\frac{1}{2}\ln\left[\frac{1+\alpha}{1-\alpha}\right]\right\} + \frac{\pi}{2} - \int_{\sqrt{n_k+1}\alpha}^{\infty}\frac{1}{1+z^2}\,dz + o\left(\frac{1}{\sqrt{n_k}}\right) = \frac{\pi}{2}.$$

Let $y = z/\sqrt{n_k+1}$. We have

$$\frac{1}{\sqrt{n_k}}\left\{\frac{1}{2}\ln\left[\frac{1+\alpha}{1-\alpha}\right] - \int_{\alpha}^{\infty}\frac{1}{\frac{1}{n_k+1}+y^2}\,dy\right\} + o\left(\frac{1}{\sqrt{n_k}}\right) = 0. \tag{43}$$

Since S_{n_k} is increasing, we have $\alpha \ge 0$. (43) implies $\alpha > 0$, otherwise the integral on the left-hand side of (43) will tend to infinity as $n_k \to \infty$. In addition, we have $\alpha < 1$, otherwise the leading term on the left-hand side of (43) will become unbounded and (43) cannot be balanced. Let $n_k \to \infty$. The leading term in (43) must satisfy

$$\frac{1}{2}\ln\left[\frac{1+\alpha}{1-\alpha}\right] - \int_{\alpha}^{\infty}\frac{1}{y^2}\,dy = \frac{1}{2}\ln\left[\frac{1+\alpha}{1-\alpha}\right] - \frac{1}{\alpha} = 0. \tag{44}$$

From this, we conclude that $S(\pi/2) = \lim_{n\to\infty} S_n(\pi/2)$ exists and $S(\pi/2) = \alpha_+$. Similarly, we can show that $S(-\pi/2) = \alpha_-$.

For $z > \pi/2$, α must take the values ± 1, otherwise (39) cannot hold for large n_k. Since S_n is increasing and $S_n \le 1$, we have $\alpha = 1$ and conclude $S(z) = 1$ for $z > \pi/2$. By a similar argument, we obtain $S(z) = -1$ for $z < -\pi/2$. The formulas for U, V, and W follow from (25) directly. The proof is complete.

We remark that U, V, W and S in the above theorem no longer satisfy second-order differential equations. Before taking the limit, U_n satisfies an equation of the from

$$0 = \frac{1}{n}d_1(U_n)_{zz} + \text{a bounded term}. \tag{45}$$

The interesting point of Theorem 5 is as follows. For an equation like (45), with its diffusion coefficient tending to zero as $n \to \infty$, one usually observes that the limit of its non-trivial solution as $n \to \infty$ has only one discontinuity across $\mathbf{R}$. However, our theorem shows that in the limit $n \to \infty$, there are two, not only one, jump discontinuities at $z = \pm\pi/2$ across $\mathbf{R}$ for our problem. To our knowledge, Theorem 5 is the first example in the literature of a reaction-diffusion system with this property.

For type-II solutions, we can also obtain a similar result as Theorem 5.

5. Concluding remarks

We investigated a three-species competition-diffusion system and used numerical methods to plot the global structures of equilibrium solutions when some parameter was varied. From this, we found that, under some conditions, stable non-constant equilibrium solutions with two humps exist. In order to obtain these solutions, we developed a semi-exact representation method. Ecologically speaking, this result indicates the coexistence of strongly competing species in the presence of an exotic competing species, from the viewpoint of competitor-mediated coexistence.

6. Appendix

We consider the problem (20) and (21). Employing a similar approach to that used in Section 4, we show in this section that the type-I and type-II solutions with a family of free parameter n presented in Section 4 can be generalized into solutions with a family of five or six free parameters. Indeed, suppose that (46) below holds.

$$r_1 = \frac{4d_1(1+k_1)^2}{k_1^2}, \qquad r_2 = \frac{4d_2(1+k_1)^2(11+5k_1)}{k_1^2},$$

$$r_3 = \frac{4d_3(1+k_1)^2(16+5k_1)}{k_1^2}, \tag{46a}$$

$$a_1 = \frac{4d_1(1+k_1)}{k_1^2}, \qquad a_2 = \frac{4d_2(11+5k_1)}{k_1^2k_2}, \qquad a_3 = \frac{54d_3}{k_1^2}, \tag{46b}$$

$$b_{12} = \frac{-4d_1(-1+k_1)}{k_1^2k_2}, \qquad b_{13} = \frac{10d_1}{k_1^2}, \tag{46c}$$

$$b_{21} = \frac{20d_2(1+k_1)(3+k_1)}{k_1^2}, \qquad b_{23} = \frac{28d_2}{k_1^2}, \tag{46d}$$

$$b_{31} = \frac{20d_3(1+k_1)(4+k_1)}{k_1^2}, \qquad b_{32} = \frac{16d_3(4+k_1)}{k_1^2 k_2}, \tag{46e}$$

$$\alpha = \frac{1}{k_1}, \tag{46f}$$

$$0 < k_1 < 1, \qquad k_2 > 0. \tag{46g}$$

We note that the free parameters in (46) are d_1, d_2, d_3, k_1, and k_2. Then Theorem 6 below follows.

THEOREM 6. *Assume that* (46) *holds. Then the problem represented by* (20) *and* (21) *admits a solution of the form*

$$\begin{cases} u(x) = k_1 + T^2(x), \\ v(x) = k_2[1 - T^2(x)]^2, \\ w(x) = [k_1 + T^2(x)][1 - T^2(x)]^2, \end{cases} \tag{47}$$

where $T = T(x)$ *is the solution of the following boundary value problem*

$$\begin{cases} \dfrac{d}{dz}T(x) = [1 - T^2(x)][1 + \alpha T^2(x)], \quad z \in \mathbf{R}, \\ T(0) = 0. \end{cases} \tag{48}$$

We remark here that when $d_1 = d_2 = d_3 = k_2 = 1$ and $k_1 = \frac{1}{n+1}$, Theorem 6 reduces to Theorem 1.

Furthermore, assume (49) below is true.

$$r_1 = 4d_1(1+m_1)^2, \qquad r_2 = \frac{2d_2(1+m_1)^2(5+7m_1)}{m_1},$$

$$r_3 = \frac{2d_3(1+m_1)^2(5+12m_1)}{m_1}, \tag{49a}$$

$$a_1 = \frac{4d_1}{k_1}, \qquad a_2 = \frac{2d_2 m_1(5+7m_1)}{k_2}, \qquad a_3 = 54d_3 m_1, \tag{49b}$$

$$b_{12} = \frac{4d_1(-4+m_1)m_1}{k_2}, \qquad b_{13} = 28d_1 m_1, \tag{49c}$$

$$b_{21} = \frac{10d_2(1+3m_1)}{k_1 m_1}, \qquad b_{23} = 28d_2 m_1, \tag{49d}$$

$$b_{31} = \frac{10d_3(1+4m_1)}{k_1 m_1}, \qquad b_{32} = \frac{6d_3 m_1(1+4m_1)}{k_2}, \tag{49e}$$

$$\alpha = m_1, \tag{49f}$$

$$k_1, k_2 > 0, \qquad m_1 > 4. \tag{49g}$$

We note that the free parameters in (49) are d_1, d_2, d_3, k_1, k_2 and m_1. Then Theorem 7 below follows.

THEOREM 7. *Suppose that* (49) *is true. Then the problem represented by* (20) *and* (21) *possesses a solution of the form*

$$\begin{cases} u(x) = k_1[1 + m_1 T^2(x)]^2, \\ v(x) = k_2[1 - T^2(x)]^2, \\ w(x) = [1 + m_1 T^2(x)][1 - T^2(x)]^2, \end{cases} \tag{50}$$

where $T = T(x)$ *is the solution of the following boundary value problem*

$$\begin{cases} \dfrac{d}{dz} T(x) = [1 - T^2(x)][1 + \alpha T^2(x)], \quad z \in \mathbf{R}, \\ T(0) = 0. \end{cases} \tag{51}$$

We remark here that Theorem 7 includes Theorem 2 as a special case in the sense that Theorem 7 becomes Theorem 2 if further conditions $d_1 = d_2 = d_3 = k_2 = 1$, $m_1 = 1 + n$, and $k_1 = \frac{1}{(1+n)(3+n)}$ are assumed.

Acknowledgement

We would like to thank Ryosuke Kon for the helpful conversation on the three-species competitive Lotka-Volterra system (1).

References

[1] M. J. Ablowitz and A. Zeppetella, Explicit solutions of Fisher's equation for a special wave speed, Bull. Math. Biol., **41** (1979), 835–840.

[2] C.-C. Chen, L.-C. Hung, M. Mimura, and D. Ueyama, Exact traveling wave solutions of three species competition-diffusion systems, to appear in Discrete and Continuous Dynamical Systems B.

[3] E. J. Doedel, B. E. Oldeman, A. R. Champneys, F. Dercole, T. F. Fairgrieve, Y. Kuznetsov, B. Sandstede, X. J. Wang, and C. H. Zhang, AUTO-07p: Continuation and bifurcation software for ordinary differential equations. Version 0.7, 2010, Concordia Univ., http://sourceforge.net/projects/auto-07p/files/auto07p

[4] S.-I. Ei, R. Ikota, and M. Mimura, Segregating partition problem in competition-diffusion systems, J. Interfaces and Free Boundaries, **1** (1999), 57–80.

[5] M. Gyllenberg and P. Yan, On a conjecture for three-dimensional competitive Lotka-Volterra systems with a heteroclinic cycle, Differential Equations and Applications, **1**(4) (2009), 473–490.

[6] M. Gyllenberg, P. Yau, and Y. Wang, A 3D competitive Lotka-Volterra system with three limit cycles: A falsification of conjecture by Hofbauer and So, Applied Mathematics Letters, **19** (2006), 1–7.
[7] T. G. Hallam, L. J. Svoboda and T. C. Gard, Persistence and extinction in three species Lotka-Volterra competitive system, Math. Biosci., **46**(1–2) (1979), 117–124.
[8] J. Hofbauer and J. W.-H. So, Multiple limit cycles for three dimensional Lotka-Volterra equations, Appl. Math. Lett., **7**(6) (1994), 65–70.
[9] Y. Kan-on, Existence of standing waves for competition-diffusion equations, Japan J. Ind. Appl. Math. **13** (1996), 117–133.
[10] Y. Kan-on, Bifurcation structure of stationary solutions of a Lotka-Volterra competition model with diffusion, SIAM J. Math. Anal. **29**(2) (1998), 424–436.
[11] Y. Kan-on, A note on the propagation speed of traveling waves for a Lotka-Volterra competition model with diffusion, J. Math. Anal. Appl. **217** (1998), 693–700.
[12] J. Kastendiek, Competitor-mediated coexistence: interactions among three species of benthic macroalgae, J. Exp. Mar. Biol. Ecol., **62**(3) (1982), 201–210.
[13] K. Kishimoto, The diffusive Lotka-Volterra system with three species can have a stable non-constant equilibrium solution, J. Math. Biol., **16**(1) (1982), 103–122.
[14] M. Rodrigo and M. Mimura, Exact solutions of a competition-diffusion system, Hiroshima Math. J. **30**(2) (2000), 257–270.
[15] M. Rodrigo and M. Mimura, Exact solutions of reaction-diffusion systems and nonlinear wave equations, Japan J. Indust. Appl. Math. **18**(3) (2001), 657–696.
[16] A. M. Turing, The chemical basis of morphogenesis, Philosophical Transactions of the Royal Society London. Series B, **237**(604) (1952), 37–72.
[17] Q. Wang, W. Huang, and H. Wu, Bifurcation of limit cycles for 3D Lotka-Volterra competitive systems, Acta Appl. Math. **114** (2011), 207–218.
[18] Wolfram Research, Inc., Mathematica, Version 5.0, Champaign, IL (2003).
[19] M. L. Zeeman, Hopf bifurcations in competitive three-dimensional Lotka-Volterra systems Dynam, Stability Systems **8**(3) (1993), 189–217.

Chiun-Chuan Chen
Department of Mathematics
National Taiwan University
Taipei, Taiwan

Li-Chang Hung
Department of Mathematics
National Taiwan University
Taipei, Taiwan

Masayasu Mimura
Graduate School of Advanced Mathematical Sciences
and Meiji Institute for Advanced Study of Mathematical Sciences
Meiji University
Kawasaki 214-8571, *Japan*

Makoto Tohma
Graduate School of Advanced Mathematical Sciences
Meiji University
Kawasaki 214-8571, *Japan*
Department of Economics
Momoyama Gakuin University
Izumi 594-1198, *Japan*
E-mail: tohma@andrew.ac.jp

Daishin Ueyama
Graduate School of Advanced Mathematical Sciences
and Meiji Institute for Advanced Study of Mathematical Sciences
Meiji University
Kawasaki 214-8571, *Japan*